Philosophical Magazine. Vol. 89. 2009. Pag. 1415-1423
http://dx.doi.org/10.1080/14786430902984566

Microstructural evolution characterization of Fe-Nb-B ternary systems processed by ball milling

BRIEF TITLE: Microstructure of ball milled Fe-Nb-B

Jhon J. Ipus[1], Javier S. Blázquez[1], Sergio Lozano-Perez[2], Alejandro Conde[1]*

[1] Departamento de Física de la Materia Condensada, ICMSE-CSIC, Universidad de Sevilla, P.O. Box 1065, 41080, Sevilla, Spain.

[2] Department of Materials, University of Oxford, Parks Road, Oxford OX1 3PH, UK.

*Corresponding author: Prof. A. Conde

Departamento de Física de la Materia Condensada. Universidad de Sevilla.

Apartado 1065, 41080 Sevilla (Spain).

Phone: (34) 95 455 28 85/ Fax: (34) 95 461 20 97

E-mail: conde@us.es

ABSTRACT: Fe-Nb-B alloys prepared by ball milling can undertake a complex microstructural evolution during milling. In order to overcome the limitations imposed by traditional X-ray bulk analysis, a comprehensive multi-technique approach was devised to systematically characterize samples with the required resolution. The combination of in-situ FIB (Focused ion beam) lift out and high resolution ATEM (Analytical transmission electron microscopy), have allowed the characterization of the phase evolution during milling. In particular, boron inclusions, not detected by X-ray diffraction, have been found to remain undissolved in the Fe matrix.

KEYWORDS: Ball milling, nanocrystalline alloys, amorphous alloys, FIB, HREM, EDX, EELS, EFTEM.

Philosophical Magazine. Vol. 89. 2009. Pag. 1415-1423
http://dx.doi.org/10.1080/14786430902984566

Introduction

Fe based amorphous and nanocrystalline alloys are very interesting due to their magnetic properties (McHenry et al, 1999), which are strongly linked with their metastable microstructure (Hernando et al, 1995). Mechanical alloying by ball milling has been shown as a very suitable and versatile technique in the production of both amorphous and nanocrystalline alloys in wide compositional ranges (Suryanarayana, 2001). Generally, mechanical alloying is developed from a starting mixture of pure powders, which progressively become alloyed to form an amorphous and/or a supersaturated solid solution. The study of microstructural evolution is frequently followed by X-ray diffraction (XRD) (Suryanarayana, 2001, Yang et al, 1996; Sherif El-Eskandarany et al, 1999; Suñol et al, 2004; Lu et al, 2006; Liu et al, 2002; Grabias et al, 2002), characterizing the phase evolution, average values of microstructural parameters (grain size and microstrains) and compositional information derived from evolution of the average lattice parameter. However, transmission electron microscopy (TEM) studies on ball milled powder samples are not so abundant (especially for magnetic materials) (Yang et al, 1996; Liu et al, 2002; Bollero et al, 2001; Liu & Chang, 2004, Du & Ramanujan, 2005,Gang et al, 2006, Han et al, 2007) due to the difficulties associated with sample preparation. TEM imaging and microanalysis supply local microstructural and compositional information overcoming the limitations of XRD. This is of special interest for the detection of minoritary phases (not only due to small volume fraction but also to low scattering power).

In this study, selected samples of Fe-Nb-B alloys prepared by ball milling were studied by different TEM imaging, diffraction and microanalysis techniques in order to obtain complementary information on the microstructure previously studied by XRD and Mössbauer spectrometry (Ipus et al, 2008).

Philosophical Magazine. Vol. 89. 2009. Pag. 1415-1423
http://dx.doi.org/10.1080/14786430902984566

Experimental

$Fe_{100-x-y}Nb_xB_y$ (x=5, y=10 and x=10, y=15) compositions were prepared from elemental powders by ball milling in a planetary mill Fritsch Pulverisette 4 Vario at 150 rpm. Details of the milling parameters can be found elsewhere (Ipus et al, 2008). For simplicity, the studied alloys will be named in the following by their Nb content: Nb10 for $Fe_{75}Nb_{10}B_{15}$ and Nb5 for $Fe_{85}Nb_5B_{10}$. Scanning electron microscopy (SEM) images obtained for short milling times show an initial mixture of the constituent elements forming heterogeneous powder particles. As an example, figure 1 shows a backscattered electron image of a powder particle for Nb10 alloy after 2 h milling at 150 r.p.m., where B particles are easily identified as dark inclusions (Ipus et al, 2008).

Different electron microscopy techniques were used in this study, including transmission (TEM), scanning transmission (STEM) and high resolution electron microscopy (HREM). Conventional bright field (BF) and dark field (DF) were used, as well as high angle annular dark field (HAADF) in STEM mode. In diffraction mode, selected area diffraction (SAD) and convergent beam electron diffraction (CBED) patterns were acquired in order to identify the different phases. Several analytical techniques were used, including energy dispersive X-ray spectroscopy (EDX), electron energy loss spectroscopy (EELS) and energy filtered transmission electron microscopy (EFTEM). Experiments were performed using three different microscopes: a Philips CM-20 operated at 200 kV, a Philips CM200 operated at 200 kV and a Jeol JEM3000F operated at 297 kV.

Sample preparation

Philosophical Magazine. Vol. 89. 2009. Pag. 1415-1423
http://dx.doi.org/10.1080/14786430902984566

The preparation of TEM specimens was performed using a FIB FEI 200, following the procedure detailed in (Lozano-Perez, 2008), applied to individual powder particles. The procedure to prepare TEM samples using FIB is schematically shown in figure 2 for a typical powder sample. The main steps followed are:

- A protective Pt layer is deposited on the surface of a selected powder particle to prevent Ga^+ damage in the region of interest during cutting and thinning processes.
- A slice of approximately 15 μm x 5 μm x 2 μm is cut from the powder particle (figure 2a-b) and welded with the help of an in-situ micromanipulator (figure 2c) to a dedicated Cu grid for TEM examination (figure 2d).
- Finally, the TEM sample is thinned to electron transparency (figure 2e-f).

Results and Discussion

Figure 3 shows BF TEM images for Nb10 alloy after 50 h milling and both alloys after 400 h milling together with a SAD pattern of the former sample. The observed microstructure for the Nb10 alloy after 50 h consists on a majority of nanocrystals with regular shape and average crystal size <D> ~10 nm (bcc-Fe type from SAD patterns in agreement with XRD results (Ipus et al, 2008)). In particular, long shaped nanocrystals (Nb rich as it will be shown later in EDX maps) and larger bright inclusions in BF images (size ~100 nm) are randomly dispersed throughout the sample. For both alloys after 400 h milling, long shaped nanocrystals do not appear and the α-Fe type nanocrystals present a smaller average crystal size, <D> ~7 nm, than that of Nb10 after 50 h milling (this agrees with XRD results, where the crystal size is just slightly reduced after 50 h milling for both alloys). Moreover, large bright inclusions (smaller

Philosophical Magazine. Vol. 89. 2009. Pag. 1415-1423
http://dx.doi.org/10.1080/14786430902984566

than for 50 h milling) are also observed. These inclusions exhibit a very weak contrast with respect to the holes in the samples, looking very bright in BF images (sometimes even saturating the negative when contrast in the nanocrystalline matrix is obtained). The brightness of these crystals in BF images could be ascribed to a low power scattering of the constituent elements of the crystals, characteristic of light elements as B, which is present in the studied alloys. Diffraction analysis evidences their crystalline nature and, moreover, lattice periodicity can be observed in HREM images.

Figure 4 (center) shows a HREM image of one of these crystalline inclusions (shown at the right) found in Nb5 after 400 h, along with the corresponding Fourier transform and image reconstruction (left). Two interplanar spacings were measured with characteristic distances of d_{hkl}=5.5 Å and 4.2 Å and an angle of ~90º. Information about crystalline structure of these crystalline inclusions can be also obtained by convergent beam electron diffraction (CBED) patterns. As an example, figure 5 shows a CBED pattern on a crystalline inclusion of the Nb5 alloy after 400 h. Interplanar distances of 5.2 Å and 3.6 Å were measured with an angle between them of 91º. B powder used in the initial mixture was characterized by X-ray diffraction and found to be β-B (JCPDF 00-031-0207). However, this phase is not consistent with the CBED and HREM results. Pure B can exhibit several allotropic structures at room temperature and, amongst them, a tetragonal structure with lattice parameters $a = b = 8.57$ Å and $c = 8.13$ Å (Taylor & Kagle, 1963) which is a plausible solution for indexing both HREM images and CBED patterns. EELS analysis suggests that some carbon was incorporated to the particle during processing (carbon contamination is an usual occurrence during ball milling using steel balls), and might explain the different crystallographic phase observed.

In addition to microstructural characterization, chemical analyses were performed for the studied samples. Figure 6, 7 and 8 show EDX compositional maps for

Philosophical Magazine. Vol. 89. 2009. Pag. 1415-1423
http://dx.doi.org/10.1080/14786430902984566

the three studied samples. For all the samples, a HAADF image is shown for identification of the different regions and individual maps of Fe, Nb and Cr (due to contamination from milling media (Ipus et al, 2008)) along with a red-green-blue (RGB) map (Fe, Nb and Cr, respectively). In the case of Nb5 after 400 h milling sample, a Pt map is also included to show the sharp edge between the Pt layer deposited during FIB sample preparation and the region of interest of the sample studied. The elemental maps have been equalized before composing the RGB image in order to enhance individual elemental contributions. For Nb10 alloy after 50 h milling, Fe and Nb are not completely mixed. The matrix formed by regular shaped nanocrystals is Fe rich and the long shaped crystals are identified as Nb rich particles. Moreover, Fe and Nb (and even Cr) free regions are observed in the EDX maps, corresponding to the bright inclusions in BF images and confirming its mainly pure B character (see corresponding HAADF image). In fact, X-rays emitted by B atoms have very low energy and cannot be efficiently detected by EDX. Besides Fe and Nb and, as expected from previous results (Ipus et al, 2008), EDX maps show the presence of Cr in the alloy due to contamination from grinding media as Cr rich clusters. It is worth mentioning the Cr-contrast between this Cr-rich cluster and the matrix, which indicates a very low Cr content in agreement with previous EDX experiments performed in SEM (below 1 at.% after 50 h milling) (Ipus et al, 2008).

Compositional maps for both alloys after 400 h milling do not show independent Fe or Nb rich regions but both elements are homogeneously dispersed throughout the samples except for those regions where Fe and Nb are not detected, ascribed to B crystals. Hence, the milling process used is unable to completely incorporate the B into the Fe(Nb) rich matrix. These B crystals, present since the starting mixture (see Fig. 1), remain for the length of the milling time explored in this study, although its size

decreases. With the milling time, homogeneous Cr content of the matrix increases in agreement with SEM results (Ipus et al, 2008) and Cr cluster are not so well defined as for the sample milled 50 h.

In order to confirm the B composition of the bright inclusions in BF images, EELS and EFTEM experiments were performed. Figure 9 shows the B content corresponding to the line profile drawn on the HAADF image obtained for Nb10 after 400 h milling. As the image provides Z-contrast, the B rich inclusion appears dark and the Fe(Nb) rich matrix appears brighter. In the inclusions, B signal is high and outside the inclusions is negligible. Figure 10 shows EFTEM images for Nb5 after 400 h milling filtered for B and Fe energies, respectively, along with the corresponding BF image for comparison. The B rich inclusion (left hand) and the Fe rich nanocrystalline matrix (right hand) can be clearly distinguished.

The observed B crystalline phase in this study by TEM was not detected using XRD in previous studies on the same samples (Ipus et al, 2008) because of the low scattering factor of B atoms. In fact, several authors studying Fe-X-B (X=Nb, Zr,…) systems achieve a final microstructure by ball milling consisting on amorphous and/or supersaturated solid solution nanocrystals without mentioning any B rich phase (Suñol et al, 2004; Lu et al, 2006; Grabias et al, 2002). On the other hand, Liu et al, 2004, detected B_2O_3 phase in Fe(Co,Ni)ZrB system submitted to ball milling. In the present study, EELS experiments do not show any significant oxygen in the B inclusions, discarding this oxide in the systems studied in this paper.

The evolution of Nb during ball milling is typical for ductile materials (Suryanarayana, 2001, Davis et al, 1988), developing long crystals with a large surface, which facilitates the incorporation of this element into the Fe nanocrystalline matrix forming a supersaturated α-Fe(Nb) solid solution. The present results do not disagree

with the preferential partitioning of Nb to intercrystalline region derived from Mössbauer results (Ipus et al, 2008). In fact, the resolution of the microscopic technique used and the sample thickness prevent any conclusion at scales below ~1 nm (intercrystalline region).

The evolution of B during ball milling is typical for brittle materials (Suryanarayana, 2001), forming inclusions which, in this case, can not be incorporated into the Fe(Nb) supersaturated solid solution. It is worth mentioning that B compounds as BN and B_4C are among the harder materials known.

Conclusions

The combination of different diffraction, imaging and analytical TEM techniques has allowed the characterization of the microstructural evolution of ball milled Fe-Nb-B alloys. While Nb and Fe followed the expected evolution during the milling process, B was found to remain undissolved for long milling times. This behavior, undetected by conventional X-ray diffraction analysis, is crucial to understand the evolution of the microstructure, the level of amorphization of the Fe matrix and some physical properties.

Acknowledgements

This work was supported by MEC of the Spanish Government and EU FEDER (Project MAT2007-65227) and the PAI of the regional Government of Andalucía (Project P06-FQM-01823). The TEM investigations were supported by the IP3 project of the 6th Framework Programme of the European Commission: ESTEEM Contract number 026019. J.J.I. acknowledges a fellowship from the Spanish Ministry of

Philosophical Magazine. Vol. 89. 2009. Pag. 1415-1423
http://dx.doi.org/10.1080/14786430902984566

Education and Science. J.S.B. acknowledges a research contract from this Regional Government.

Philosophical Magazine. Vol. 89. 2009. Pag. 1415-1423
http://dx.doi.org/10.1080/14786430902984566

Figure legends

Figure 1. Back scattered SEM image showing B inclusions (dark particles) in a typical powder of Nb10 alloy after 2 h milling.

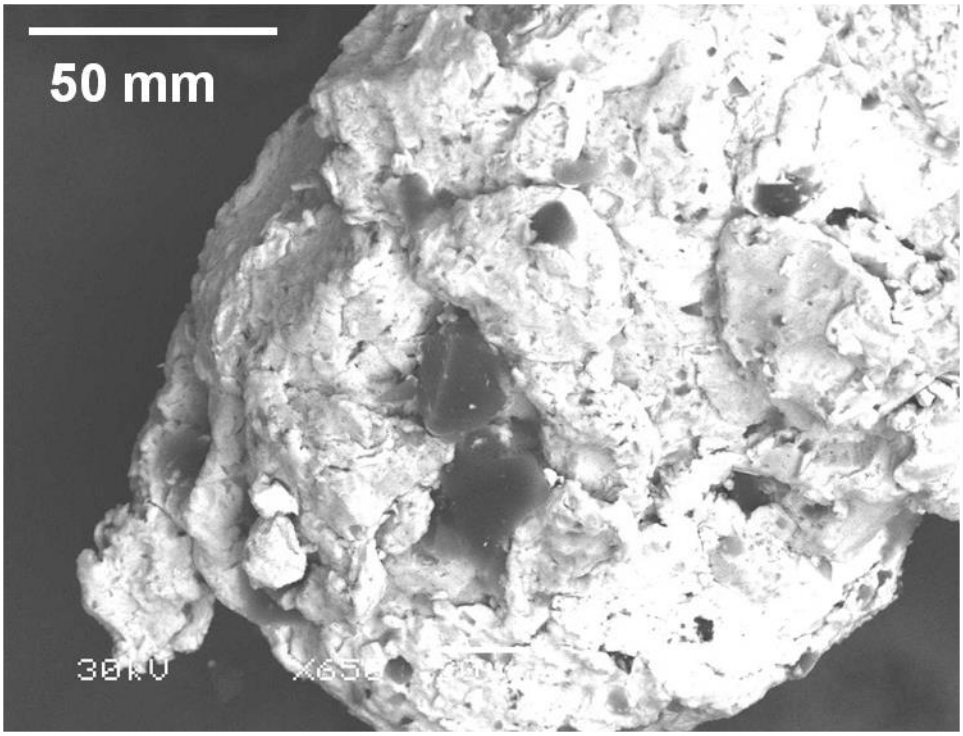

Philosophical Magazine. Vol. 89. 2009. Pag. 1415-1423
http://dx.doi.org/10.1080/14786430902984566

Figure 2. Images of the TEM sample preparation using FIB. In situ images from secondary electrons: a) and b) cutting of a powder particle after Pt layer deposition, c) sample welded to the micromanipulator, d) sample welded to the TEM sample holder and cut from the manipulator and e) sample thinned. Finally, f) TEM BF image of the Nb10 after 50 h milling sample showing B inclusions.

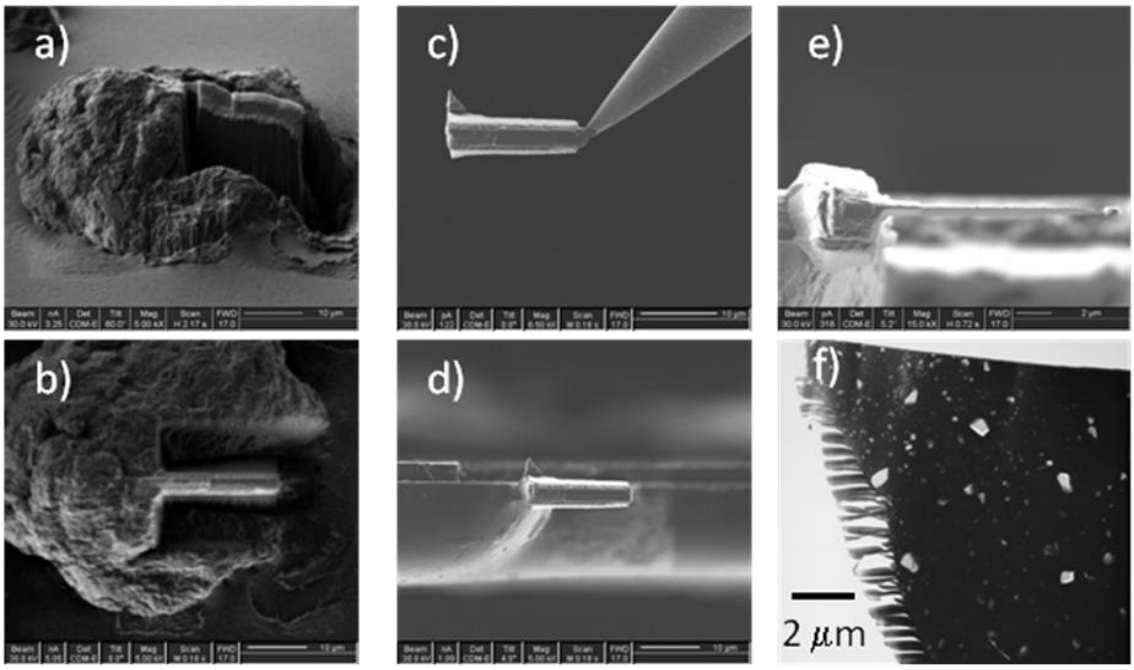

Figure 3. From left to right SAD image of Nb10 after 50 h milling and BF TEM images of Nb10 after 50 h milling, Nb10 after 400 h milling and Nb5 after 400 h milling. The scale bar is common to the three BF images.

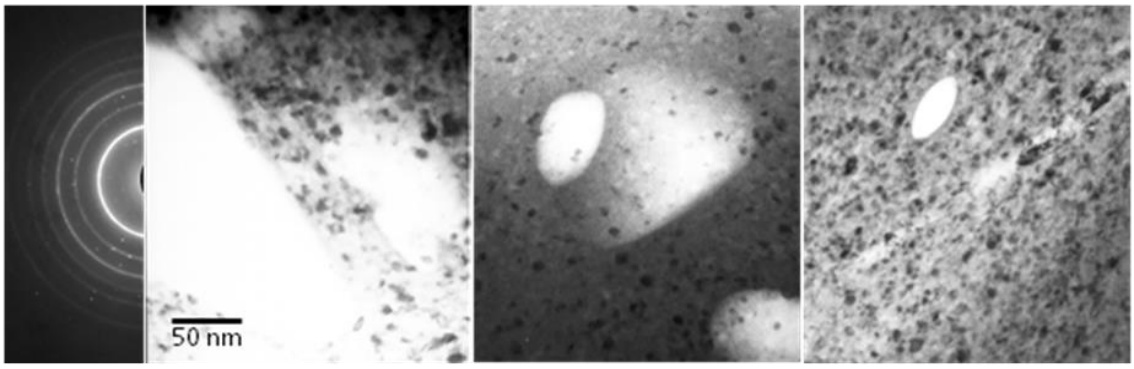

Philosophical Magazine. Vol. 89. 2009. Pag. 1415-1423
http://dx.doi.org/10.1080/14786430902984566

Figure 4. From left to right: BF image of Nb5 after 400h showing a B inclusion and the Pt layer (left), HREM of the B inclusion and corresponding Fourier transform with image reconstruction.

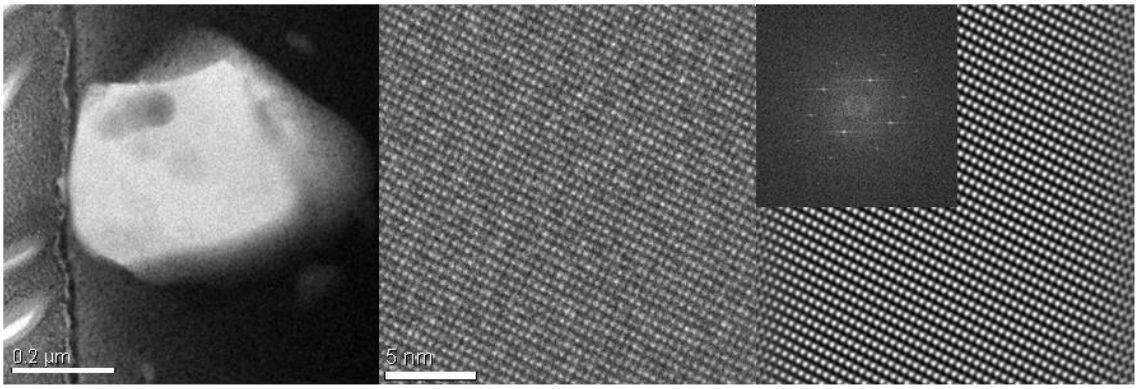

Figure 5. CBED pattern of a B rich inclusion obtained for Nb5 alloy after 400 h milling and plausible indexation using a tetragonal crystalline structure with a=8.57 and c=8.13 Å corresponding to a [1 1 1] zone axis were (-1 0 1) with d=5.898 Å and (-1 2 -1) with d=3.467 Å form an angle of 91.77º.

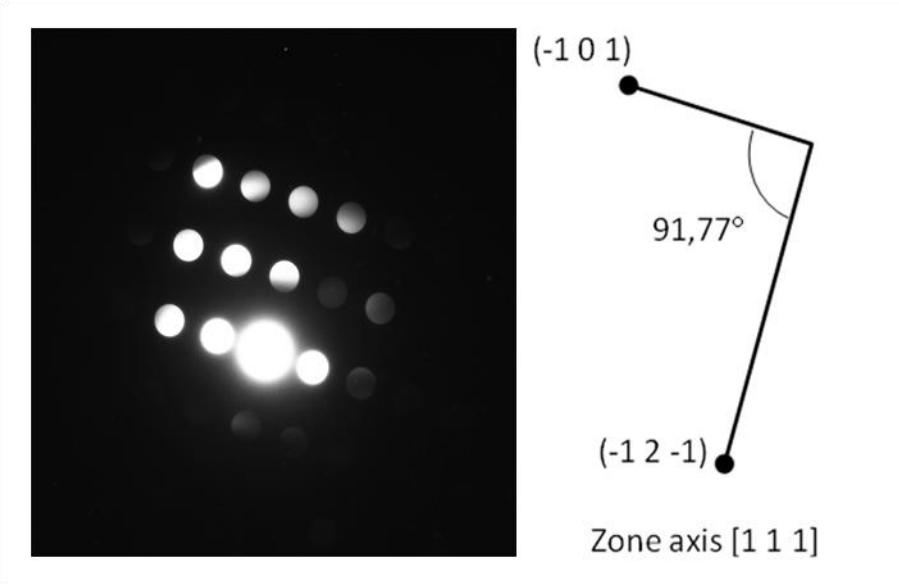

Philosophical Magazine. Vol. 89. 2009. Pag. 1415-1423
http://dx.doi.org/10.1080/14786430902984566

Figure 6. HAADF image and EDX maps of Nb10 alloy after 50h milling using K line for Fe, K plus L lines for Nb and K line for Cr. Red, green and blue correspond to Fe, Nb and Cr, respectively in the RGB colored map.

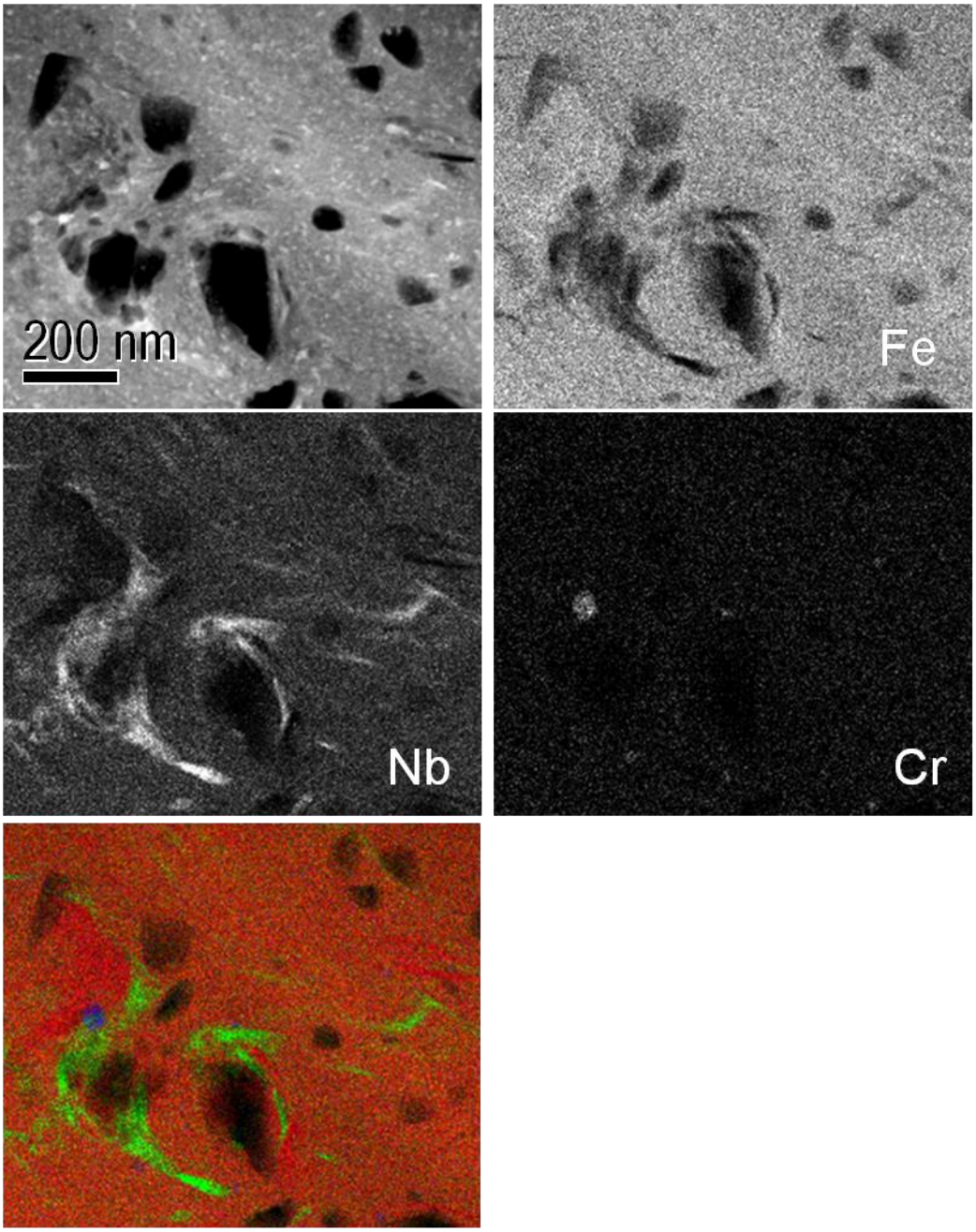

Philosophical Magazine. Vol. 89. 2009. Pag. 1415-1423
http://dx.doi.org/10.1080/14786430902984566

Figure 7. HAADF image and EDX maps of Nb10 alloy after 400h milling using K line for Fe, K plus L lines for Nb and K line for Cr. Red, green and blue correspond to Fe, Nb and Cr, respectively in the RGB colored map.

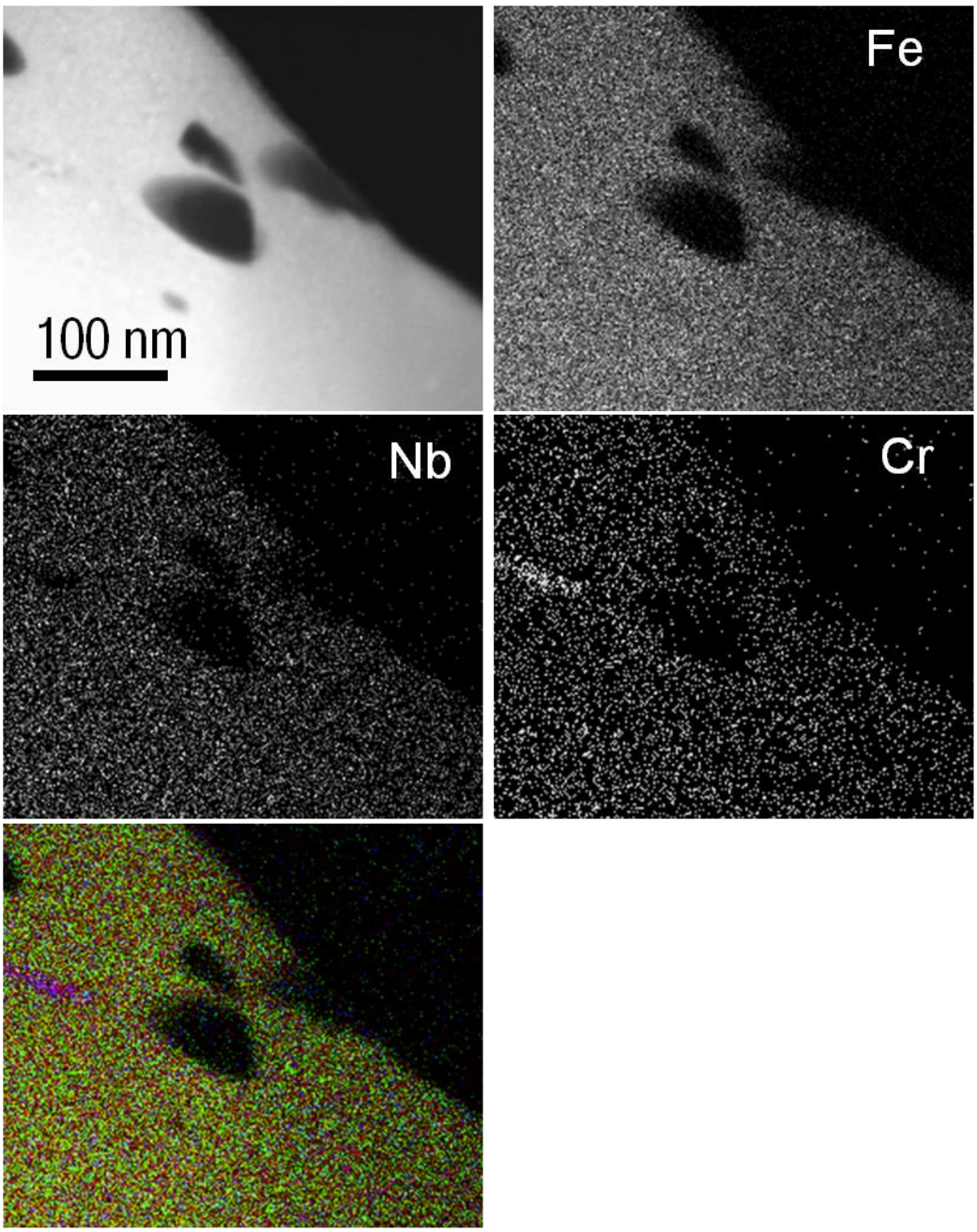

Philosophical Magazine. Vol. 89. 2009. Pag. 1415-1423
http://dx.doi.org/10.1080/14786430902984566

Figure 8. HAADF image and EDX maps of Nb5 alloy after 400h milling using K line for Fe, K plus L lines for Nb, K line for Cr and L line for Pt, showing the clear separation between the sample of interest and the Pt protective layer deposited during TEM sample preparation. Red, green and blue correspond to Fe, Nb and Cr, respectively in the RGB colored map.

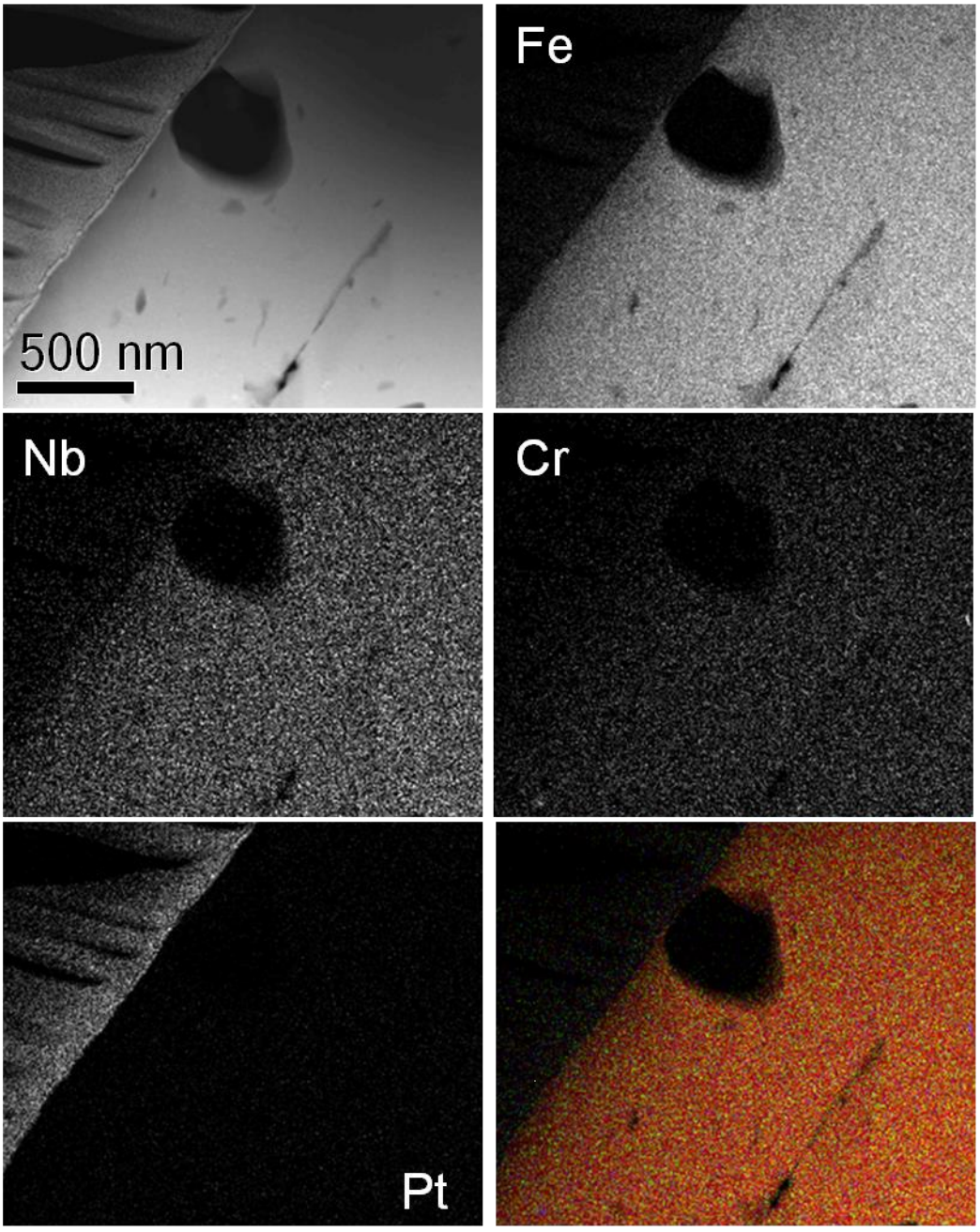

Philosophical Magazine. Vol. 89. 2009. Pag. 1415-1423
http://dx.doi.org/10.1080/14786430902984566

Figure 9. HAADF image of Nb10 alloy after 400h and B profile corresponding to the line drawn in the image obtained by EELS.

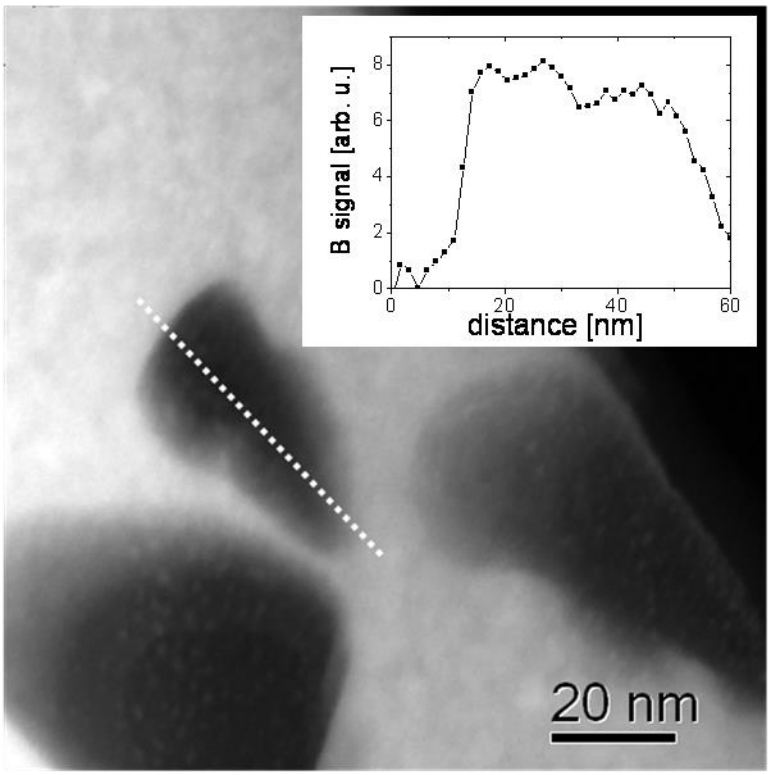

Figure 10. BF image and EFTEM images acquired at the characteristic energies of B and Fe of Nb5 alloy after 400h showing a B inclusion (left), the nanocrystalline matrix (right) and the Pt protective layer (below).

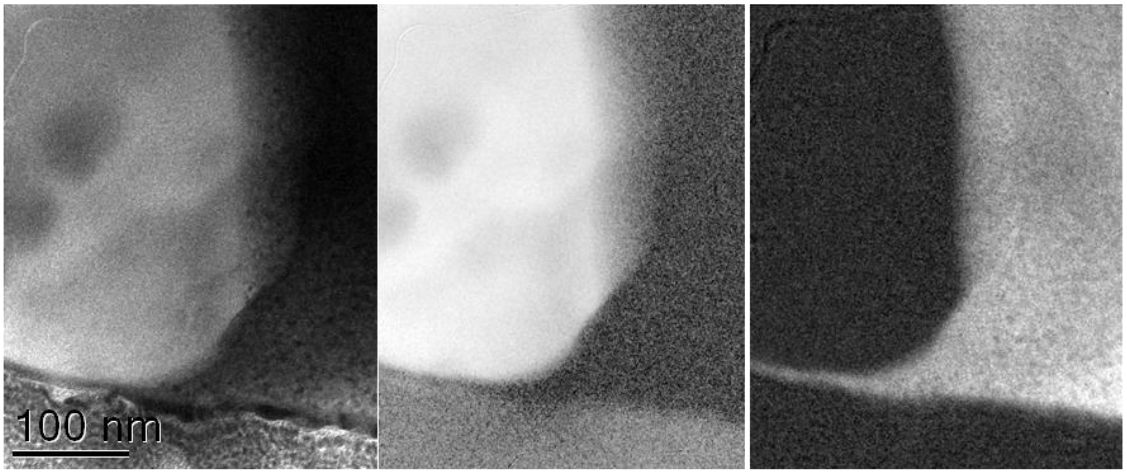

Philosophical Magazine. Vol. 89. 2009. Pag. 1415-1423
http://dx.doi.org/10.1080/14786430902984566

References

- Bollero A., Gebel B., Gutfleisch O., Müller K.H., Schultz L., McGuiness P.J., Drazic G., Kobe S. (2001). NdDyFeBZr high-coercivity powders prepared by intensive milling and the HDDR process *J. All. Compd.* **315**, 243-250.
- Davis R.M., McDermott B., Koch C.C. (1988). Mechanical alloying of brittle materials. *Metall. Trans. A.* **19**, 2867-2873.
- Du S.W., Ramanujan R.V. (2005). Mechanical alloying of Fe–Ni based nanostructured magnetic materials, *J. Mag. Mag. Mat.* **292,** 286-298.
- Gang S., Lianxi H., Erde W. (2006). Preparation, microstructure, and magnetic properties of a nanocrystalline Nd12Fe82B6 alloy by HDDR combined with mechanical milling, *J. Mag. Mag. Mat.* **301**, 319-324.
- Grabias A., Kopcewicz M., Oleszak D. (2002). Phase transformations in the Fe(Co,Ni)ZrB alloys induced by ball milling. *J. All. Compd.* **339**, 221-229.
- Han J., Lui S., Zang X., Du H., Wang C., Yang Y., Yue M., Liu X. (2007) Equiaxed Nd-Fe-B fine powder with high performance prepared by mechanical alloying. *J. Appl. Phys.* **101,** 09K502.
- Hernando A., Vázquez M., Kulik T., Prados C. (1995). Analysis of the dependence of spin-spin correlations on the thermal treatment of nanocrystalline materials. *Phys. Rev. B* **51**, 3581- 3586.
- Ipus J.J., Blázquez J.S., Franco V., Conde A. (2008). Mechanical alloying of Fe100−x−yNbxBy (x = 5, 10; y = 10, 15): From pure powder mixture to amorphous phase. *Intermetallics* **16,** 1073-1082.
- Liu Y.J., Chang I.T.H. (2002). Compositional dependence of crystallization behavior of mechanically alloyed amorphous Fe-Ni-Zr-B alloys. *Mater. Sci. Eng. A* **325**, 25-30.

- Liu Y.J., Chang I.T.H. (2004). Effects of oxide phases on thermomagnetisation of mechanically alloyed amorphous Fe–(Co, Ni)–Zr–B powder. *Mater. Sci. Eng. A* **375-377,** 1092-1096.
- Lozano-Perez S. (2008) A guide on FIB preparation of samples containing stress corrosion crack tips for TEM and atom-probe analysis. *Micron* **39,** 320-328.
- Lu W., Yang L., Yan B., Huang W., Lu B. (2006). Nanocrystalline Fe84Nb7B9 alloys prepared by mechanical alloying and ultra-high-pressure consolidation. *J. All. Compd.* **413**, 85-89.
- McHenry M.E., Willard M.A., Laughling D.E. (1999). Amorphous and nanocrystalline materials for applications as soft magnets. *Prog. Mat. Sci.* **44**, 291-433.
- Sherif El-Eskandarany M., Bahgat A.A., Gomaa N.S., Eissa N.A. (1999). Kinetics and formation mechanism of amorphous Fe52Nb48 alloy powder fabricated by mechanical alloying. *J. All. Compd.* **290,** 181-190.
- Suñol J.J., Gonzalez A., Saurina J., Escoda Ll., Bruna P. (2004). Thermal and structural characterization of Fe–Nb–B alloys prepared by mechanical alloying. *Mater. Sci. Eng. A* **375-377**, 874-880.
- Suryanarayana C., (2001). Mechanical alloying and milling. *Prog. Mat. Sci.* **46,** 1-184.
- Taylor A., Kagle B. J. (1963). Crystallographic data on metal and alloy structures, p. 254, New York, USA: Dover.
- Yang J.Y., Zhang T.J., Cui K., Li X.G., Zhang J. (1996). Amorphization of Fe_Nb by mechanical alloying. *J. All. Compd.* **242**, 153-156.